The effect of sample anisotropy properties, dimensions, and imposed no-flow boundaries on the measurement of directional permeability and viscous resistivity

Jacob McGregor[1,*]

[1]Halliburton, Jet Research Center, Alvarado, TX, USA

Abstract. The mathematical theory underpinning the permeability measurement on homogeneous anisotropic porous media is reviewed. The effect of sample anisotropy properties, dimensions, and imposed no-flow boundaries on the directional permeability measurement, and its reciprocal—the directional viscous resistivity—are discussed and illustrated graphically through numerical simulation. In general, the directions of the specific discharge and potential gradient vectors are not collinear, and therefore two different definitions are possible for the directional permeability, each yielding a different value for a given set of conditions, and significantly different values for different sample diameter-length ratios (D/L). However, it is shown that the one and only directional permeability as dictated by the three-dimensional form of Darcy's law is the permeability in the direction of the potential gradient $k_\Phi = k_{ij}u_iu_j = k$, which requires a sample geometry of $D/L = \infty$. In practice, it is an apparent directional permeability k_a that is measured on a finite dimensioned sample, and thus a sample geometry of $D/L \gg 1$ is required to approximate k_Φ. This geometry is contrary to what is generally used and recommended to measure permeability, $D/L \leq 1$, resulting in sometimes significant error. It is shown that the apparent directional viscous resistivity r_a is what is to be measured when sample D/L geometries < 1 are being evaluated and its measurement accuracy improves as $D/L \to 0$. The relations between the measured k_a and r_a of a cylindrical three-dimensional sample and its D/L, k_{ij}, r_{ij}, and u_i properties are presented. Approximate analytical solutions for k_a and r_a are provided, which can be used to guide choice of experimental setup and to approximate measurement accuracy. An extended definition for the unit of directional permeability for anisotropic flow is provided based on this work.

1 Introduction

The fundamental law of fluid flow through porous media as given by Darcy [1] assumes the porous medium to be isotropic in permeability; the permeability parameter was represented as a single scalar quantity. Ferrandon [2] theoretically showed that for the case of anisotropic media, permeability is a material tensor of second rank. Nye [3] provided the experimental methodology for measuring the magnitude of an anisotropic parameter in a particular direction, taking into consideration sample dimensions and boundary conditions. Bear [4] (p.148), provides the principle (and steps) underlying the experimental determination of coefficients appearing in the macroscopic description of phenomena (e.g., the permeability and viscous resistivity coefficients of Darcy's law) – where emphasis is placed on understanding the flow pattern of the experiment and if it permits the desired coefficient to be measured. This paper seeks to marry these two ideas given by Nye and Bear. To do so, numerical flow simulations were conducted and analyzed under the guise of Nye and Bear, the results from which can be used to guide physical experimental work for determining the permeability and viscous resistivity coefficients of Darcy's law.

2 Background

The issue of measuring permeability of an anisotropic sample of finite dimension using a conventional "axial" permeameter [5], where boundaries must be imposed, was investigated by Marcus and Evenson [6] and Marcus [7]. As noted by Bear [4] (p.146), "it becomes obvious that knowledge of both k_{ij} (e.g., by knowing the principal values k_1, k_2, and k_3, and the principal directions) and the boundary conditions is required to determine the flow pattern. This conclusion has an important bearing on the determination of permeability by permeameters in anisotropic media." Much has been published on the theory of anisotropic permeability. More generally, the mathematical theory of matter tensors and their laboratory determination has been discussed in detail in literature outside the field of fluid flow in porous media, e.g., see [3, 8, 9]. Hydraulic resistivity R is the reciprocal of hydraulic conductivity K [4] (p.140). Viscous resistivity r is the reciprocal of permeability k ([10] (p.6-1, Sec. 6.1); [11] (p.10, Sec. 2.4)). These coefficients and their measurement have been discussed to a lesser extent in porous media literature. The following three background subsections contain material mostly given in Nye, material that will set the stage for the experimental work and analysis given in this paper. The material is limited to the key points that will be

used to support the analysis and discussion of this work and is provided for completeness. Following the third subsection is a note on the significance of what is said in these three background subsections.

2.1 The magnitude of a second-rank tensor and its geometric interpretation

The scalar magnitude S of a symmetrical second-rank tensor S_{ij} in a specific direction defined by a unit vector u_i is found by contracting the unit vector with the indices of S_{ij} as shown in Equation (1) [3] (p.26)

$$S = S_{ij}u_iu_j. \tag{1}$$

The tensor S_{ij} relates the respective force-flux (cause-effect) vectors b_j and a_i to each other by the matrix product,

$$a_i = S_{ij}b_j. \tag{2}$$

Invoking Equation (2) into Equation (1), we find the geometrical relationship between the magnitude of S_{ij} and vectors a_i and b_j,

$$S = S_{ij}u_iu_j = \frac{S_{ij}b_jb_i}{|b_i|^2} = \frac{a_i \cdot b_i}{|b_i|^2}$$
$$= \frac{|a_i||b_i|\cos(\theta)}{|b_i|^2} = \frac{|a_i|\cos(\theta)}{|b_i|}, \tag{3}$$

where θ is the angle between vectors a_i and b_j. Equation (3) states that the magnitude S characterizing S_{ij} in a specific direction is the ratio of the scalar projection of vector a_i onto this direction to the magnitude of the vector b_i. Equation (3) also instructs how the magnitude S of the property S_{ij} in a specific direction is to be obtained experimentally — apply b_i in that direction and measure $a_\parallel/|b_i|$, where $a_\parallel = |a_i|\cos\theta$ is the component of a_i parallel to b_i.

2.2 The Permeability and Viscous Resistivity Tensor

Darcy's law for the flow of a single-phase incompressible Newtonian fluid through a porous medium is

$$q_i = K_{ij}J_j = -K_{ij}\partial h/\partial x_j = -\mu^{-1}k_{ij}\partial\Phi/\partial x_j, \tag{4}$$

where k_{ij} is the symmetrical second-rank permeability tensor and $i,j = 1,2,3$, corresponds to the direction of the coordinate axes x, y, z. (See nomenclature for definitions of other variables). Equation (4) may be solved for the $\partial\Phi/\partial x_j$ in terms of the viscus resistivity tensor r_{ij}

$$-\partial\Phi/\partial x_i = \mu r_{ij}q_j. \tag{5}$$

The viscous resistivity tensor r_{ij} is the reciprocal of the permeability tensor, determined through Equation (6)

$$r_{ij} = k_{ij}^{-1} = \text{cofactor of } k_{ij}/\det k_{ij}. \tag{6}$$

2.3 Experimental Measurement of Permeability and Viscous Resistivity

Consider Darcian flow through two right-circular cylinder-shaped porous solids with different diameter to length ratios (D/L). The porous solids are macroscopically homogeneous and anisotropic with respect to permeability. The cylinders are of the same porous solid and have k_{ij} in the same orientation, that is, they are identical in every way except for their diameter to length ratio. In the following descriptions

and illustrations, the gravitational acceleration vector g_i is collinear with the x_1 axis.

Figure 1A shows a relatively large-diameter and short-length sample $(D/L \gg 1)$, i.e., a "thin-disc", between two flow distributor plates. The fluid potential at the inlet plate is greater than the fluid potential at the outlet plate. Since the sample is of large cross section compared with its length, the isopotential surfaces must run parallel to the planar end faces of the porous medium apart from edge effects near the outer cylindrical surface — over the region roughly outlined by the dashed line. The fluid potential gradient vector is therefore prescribed to be perpendicular to the end faces, and the specific discharge vector, is in general, oriented in some other direction due to the sample's anisotropic permeability (the flow will take the path of least resistance). Since it is the direction of $-\partial\Phi/\partial x_i$ rather than q_i that is prescribed in this experiment, it is better to work with permeabillities than with viscous resistivities; from Equation (4) we write,

$$q_i = -\mu^{-1}k_{i1}\partial\Phi/\partial x_1, \tag{7}$$

where x_1 is taken to be perpendicular to the sample's end faces. According to Equation (3) the component of q_i parallel to $-\partial\Phi/\partial x_1$ needs to be measured. If done so, k_{11} is the quantity most readily measured in this experiment.

Figure 1B shows a relatively small-diameter and long-length sample $(D/L \ll 1)$, i.e., a "long rod", between two flow distributor plates. The cylindrical surface of the sample is sealed by an impermeable barrier. In this case, the specific discharge vector must be compelled along the cylinder's long axis (aside from effects at the end faces in the region roughly outlined by the dashed line). However, with such boundaries the orientation of the potential gradient vector is unknown, the isopotential surfaces are generally oblique to the cylinder's long axis due to the sample's anisotropic permeability. Since the direction of q_i is prescribed to be parallel to x_1 it is now better to work with viscous resistivities. Thus, from Equation (5) we write,

$$-\partial\Phi/\partial x_i = \mu r_{i1}q_1. \tag{8}$$

The component of the fluid potential gradient along the length of the sample, which is what would be most easily measured in the experiment, is $-\partial\Phi/\partial x_1$. Since $-\partial\Phi/\partial x_1 \equiv (-\partial\Phi/\partial x_i)_\parallel$, where $(-\partial\Phi/\partial x_i)_\parallel$ is the component of $-\partial\Phi/\partial x_i$ parallel to q_i, then r_{11} is the quantity most readily measured in this experiment.
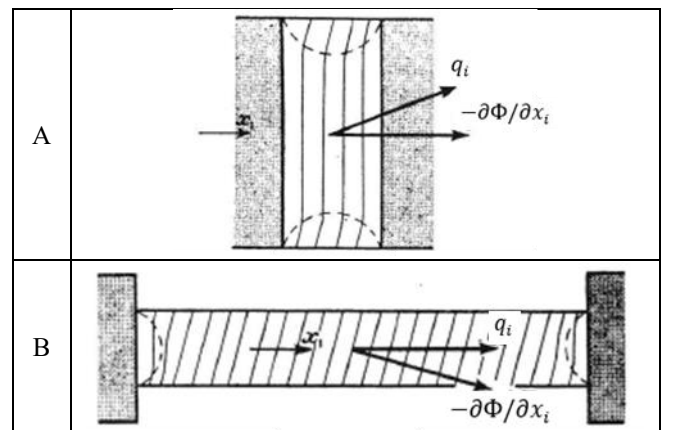
Figure 1. Fluid flow through (A) a large-diameter and short-length cylindrical core, illustrated with isopotentials and regions where cylindrical-edge effect occurs, and (B) a small-diameter and long-

length cylindrical core, illustrated with isopotentials and regions where planar-end effect occurs (modified and sourced from [3]).

The above description and figures parallels what is found in [3] (pp.213-216), [8] (pp.37-40), and [9] (pp.203-206). However, after reading the above description the following questions come to mind:

I. Should the cylindrical surface of the thin-disc testing (for measuring permeability) be sealed by an impermeable barrier or not? Based on the description given—which does not explicitly state to have the cylindrical surface sealed by an impermeable barrier in [3, 8, and 9]—it might seem that the cylindrical surface should not be sealed and only the flow that exits the outlet planar face should be taken as q_1. Otherwise, if the cylindrical surface was made to be sealed to flow, the components of the specific discharge vector in the x_2 and x_3 directions will be diverted to the x_1-direction and included in the flow measurement. Hence, the ratio of the total flow (in all directions) to the potential gradient (prescribed to be oriented along the x_1-direction) would be computed instead.

II. How do the fluid potential contours and specific discharge vector field change as a function of sample dimension?

III. How does the permeability and viscous resistivity value change as a function of sample dimension?

IV. What does it mean to be "relatively large-diameter and short-length sample", "of large cross section compared with its length", and "a relatively small-diameter and long-length sample"?

A series of numerical simulations were conducted to address these questions. Before describing the numerical simulations, a comment to the significance of the statements made in these background sections is warranted.

2.4 Significance of Statements Made in Sections 2.1 through 2.3

To compare the second-rank permeability tensor of Equation (4) with the scalar value determined from physical measurements, Scheidegger [12,13] introduced the notion of a "directional permeability". In doing so, Scheidegger defined two kinds of scalar directional permeabilities, a "permeability in the direction of flow",

$$k_q = \frac{\mu|q_i|}{|\partial\Phi/\partial x_i|\cos(\theta)} = -\frac{\mu|q_i|}{\partial\Phi/\partial x_i \cdot m_i}, \quad (9)$$

where θ is the angle between vectors q_i and $-\partial\Phi/\partial x_i$ and m_i is a unit vector in the direction of the q_i, and a permeability in the direction of the fluid potential gradient,

$$k_\Phi = \frac{\mu|q_i|\cos(\theta)}{|\partial\Phi/\partial x_i|} = \frac{\mu q_i \cdot n_i}{|\partial\Phi/\partial x_i|}, \quad (10)$$

where n_i is a unit vector in the direction of the negative of the potential gradient[1]. The "permeability in the direction of flow" corresponds to what would be measured using sample dimensions and boundary conditions described for the "long rod" experiment described in Section 2.3, Figure 1B;

the "permeability in the direction of the fluid potential gradient" corresponds to the "thin disc" experiment, Figure 1A. Strictly, k_q and k_Φ are limiting expressions of what would be measured in a conventional axial permeameter where boundary conditions are imposed, in the limit that sample dimensions $D/L \to 0$ and $D/L \to \infty$, respectively. These two values are the extremes, and the actual conventionally measured permeability of a finite-dimensioned sample is called the apparent permeability $k_a = Q\mu L/(A\Delta\Phi)$, whose value will generally fall between the two extremes k_q and k_Φ.

The values of these two directional permeabilities, as defined, are not the same unless measurements are made with q_i and $-\partial\Phi/\partial x_i$ in the direction of one of the permeability tensor's principal axes. Scheidegger [13] (p.65) stated that, "The fact that there are two different kinds of 'directional permeability,'… is somewhat disconcerting." However, this issue may be alleviated. The mathematical structure of Equations (2) and (4) are analogous, therefore, Equation (3) provides the one and only relationship that should define the scalar directional permeability, which is Equation (10) – the "permeability in the direction of the fluid potential gradient" k_Φ. Explicitly,

$$k = k_{ij}u_iu_j = \frac{\mu|q_i|\cos(\theta)}{|\partial\Phi/\partial x_i|} = \frac{\mu q_i \cdot n_i}{|\partial\Phi/\partial x_i|} = k_\Phi. \quad (11)$$

The scalar directional permeability defined by Equation (10) relates to the components k_{ij} of the permeability tensor as shown in Equation (11). Since the permeability tensor is defined by Darcy's law, Equation (4), three points are of note:

1. The permeability tensor is a linear operator that operates on the potential gradient vector to produce a specific discharge vector (Equation (4)).

2. The term "permeability" is defined by Darcy's law [15] (p.10), which refers to the magnitude of the fluid potential gradient vector and the component of the specific discharge vector colinear with it (Equation (10)).

3. The unit of permeability is defined by Darcy's law. That is, a material has a *directional permeability* of one darcy if through a face of one square centimeter, *which is normal to the direction of the potential gradient*, one cubic centimeter per second of fluid having viscosity one centipoise is caused to flow by a potential gradient of one atmosphere per centimeter.

Thus, it is the "thin disc" experiment, where the diameter of the sample (core) is relatively large and length is relatively short $(D/L \gg 1)$, that permits the measurement of permeability. However, this disagrees with recent literature concerning the recommended practice for measuring permeability (and with Darcy's experiments, where the D/L ratios for his sand packs ranged from 0.6 to 0.2, and possibly as low as 0.13 [16,17]). For example, [18] recommends testing samples with a length between 1.3 and 1.7 times the diameter of the sample. According to [19] (p.106), "Most routine and special core analysis tests are performed on plug samples cut from the full diameter core. The plug samples are

---

[1] The notion of two kinds of scalar directional permeabilities stemming from the permeability tensor is not isolated to porous media. The "conductivity in the direction of the flux vector" and the

"conductivity normal to the isothermals" have been defined in the exact same manner in the study of conduction of heat in anisotropic solids [14] (pp.38-49).

right cylinders typically 1- or 1.5-inches in diameter and 1-3-inches long. The rule of thumb is that the plugs for RCA or SCAL should have a length equivalent to one to two times the plug diameter." This rule of thumb for dimensions can lead to a D/L ratio as low as 0.5 and at most a ratio of 1. Indeed, as noted in [10] (Section 6.3.1.1.1.1), core plugs having either a 1.0- or 1.5-inch diameter, 0.75- to 3-inch length are dimensions that have become virtually standard in conventional analysis. This range of dimensions can lead to a D/L ratio as low as 0.33 and at most a ratio of 2.

The so-called scalar directional "permeability in the direction of flow", k_q, is related to k_{ij} and r_{ij} as shown in Equation (12),

$$k_q = \frac{\mu|q_i|}{|\partial\Phi/\partial x_i|\cos(\theta)} = -\frac{\mu|q_i|}{\partial\Phi/\partial x_i \cdot m_i}$$
$$= \frac{1}{k_{ij}^{-1}m_i m_j} = \frac{1}{r_{ij}m_i m_j}. \qquad (12)$$

If the goal is to measure values to be used in Darcy's law while employing the "long rod" experiment, then, the directional viscous resistivity in the direction of flow r_q is the value to be measured, not k_q, and used in Darcy's law written in viscous resistivity form, Equation (8). Explicitly, the relations for r_q are,

$$r = r_{ij}u_i u_j = \frac{|\partial\Phi/\partial x_i|\cos(\theta)}{\mu|q_i|}$$
$$= \frac{-\partial\Phi/\partial x_i \cdot m_i}{\mu|q_i|} = r_q. \qquad (13)$$

Scheidegger's two directional permeabilities can lead to confusion and error due to the use of the name "permeability" for the value k_q. In the general case where one does not know the orientations of principal permeabilities for the sample that they are measuring, one should not try to determine values for k_{ij} when measuring k_q using the "long rod" experiment and subsequently use these k_{ij} values in Darcy's law, Equation (4). Rather, the correct procedure would be to measure six or more values of r_q using the "long rod" experiment (see Appendix), determine values for r_{ij} and either use these values in the viscous resistivity form of Darcy's law, Equation (5), or determine k_{ij} by taking the reciprocal of r_{ij} and using these k_{ij} in the permeability form of Darcy's law, Equation (4). This is important for "highly" anisotropic samples. An example of this procedure is provided in Section 4.III, Figure 14.

As noted by [20], to avoid the difficulty of selecting the experimental setup and employing the correct corresponding analysis, "most measurements are made parallel or perpendicular to the bedding plane with the direction perpendicular to the bedding plane being *assumed* to be one of the principal directions. Measurements are made at all angles parallel to the bedding plane and the maximum and minimum permeabilities in this plane, if perpendicular, are *assumed* to be the principal permeability components in that plane. *The direction of the bedding plane, however, does not necessarily have to correspond to a principal direction of the specimen, a situation which complicates the interpretation of the measurements.*" (Emphasis added). This statement also assumes the sample has visually identifiable bedding or bedding at all. Therefore, to avoid having to make assumptions and to avoid having to face complicated

interpretations, one should determine permeability $k(= k_\Phi)$ using the thin disc experiment, and viscous resistivity $r(= r_q)$ using the long rod experiment; from which k_{ij} and r_{ij} can be determined (see Appendix). Lastly, with the apparent permeability k_a now defined, questions III and IV can be combined and refined to the following, similar to how [7] had posed: What dimensions does the sample need to have to yield k with a certain desired accuracy or, more generally, what is the relation between the geometry of a cylindrical sample, expressed by the D/L ratio, and the apparent permeability k_a for a given anisotropy k_{ij} and orientation u_i? The same can be asked for r, where $r_a = A\Delta\Phi/(Q\mu L)$.

3 Description of the Numerical model

For the three-dimensional simulations the cylindrical core's main (symmetrical) axis was made to be collinear with the right-handed Cartesian (x, y, z) x-axis as depicted in Figure 2. The principal values of the permeability tensor (denoted as k'_{ij}; $i = x', y', z'$) were defined as

$$k'_{ij}\,(x', y', z') = \begin{bmatrix} 20 & 0 & 0 \\ 0 & 1 & 0 \\ 0 & 0 & 1 \end{bmatrix}\text{ md.} \qquad (14)$$

The permeability tensor for the core is geometrically represented as an ellipsoid in Figure 2. With k'_{ij} initially coordinate-axis-aligned (Figure 2A), it was rotated using a rotation matrix R_{ij} [21], rotated with respect to the core's (fixed) xyz coordinate system (Figure 2B), according to

$$k_{mn} = R_{mi}R_{nj}k'_{ij} \qquad (15)$$

It was desired to have the maximum principal permeability axis orientated at a +45° angle α (positive counterclockwise) from the x-axis, and one of the two identical intermediate and minimum principal permeability axes collinear with the z-axis. The symmetry of this system permits the three-dimensional flow simulation results to be understood when viewed in a two-dimensional view (in the x-y plane) as conceptually illustrated in Figure 2C. To achieve the desired tensor orientation (as depicted in Figure 2), the rotation matrix was defined through three successive rotations according to the so-called Roe convention [21], which consists of a rotation through angle ψ about the z-axis, then a rotation of angle θ about the new y-axis (which has already rotated itself due to the first rotation about the z-axis), and finally, a second rotation of ϕ about the now-tilted z-axis. The rotation matrix as a product of these three successive rotations is then

$$R_{ij} = \begin{bmatrix} c\psi\,c\theta\,c\phi - s\psi\,s\phi & -c\psi\,c\theta\,s\phi - s\psi\,c\phi & c\psi\,s\theta \\ s\psi\,c\theta\,c\phi + c\psi\,s\phi & -s\psi\,c\theta\,s\phi + c\psi\,c\phi & s\psi\,s\theta \\ -s\theta\,c\phi & s\theta\,s\phi & c\theta \end{bmatrix}, (16)$$

where c and s are trigonometric functions cosine and sine, respectively. For other conventions see [22]. For the desired tensor orientation, the Roe angles required are: $\psi = 45°$; $\theta = 0°$; $\phi = 0°$, which results in the rotation matrix:

$$R_{ij} = \begin{bmatrix} \sqrt{2}/2 & -\sqrt{2}/2 & 0 \\ \sqrt{2}/2 & \sqrt{2}/2 & 0 \\ 0 & 0 & 1 \end{bmatrix}. \qquad (17)$$

Invoking Equations (14) and (17) into Equation (15), the permeability tensor used in the simulations is then,

$$k_{ij}(x, y, z) = \begin{bmatrix} 10.5 & 9.5 & 0 \\ 9.5 & 10.5 & 0 \\ 0 & 0 & 1 \end{bmatrix} \text{md.} \qquad (18)$$

The main (symmetry) axis of the core is made to be aligned with the x-axis in the simulations as depicted in Figure 2, which is an orientation defined by the unit vector $u_i = [1, 0, 0]$. Thus, from Equation (1), the magnitude of the permeability tensor along the x-axis is 10.5 md. The magnitude of the viscous resistivity tensor along the x-axis is found by taking the reciprocal of the permeability tensor [see Equation (6)],

$$r_{ij}(x, y, z) = \begin{bmatrix} 0.525 & -0.475 & 0 \\ -0.475 & 0.525 & 0 \\ 0 & 0 & 1 \end{bmatrix} \text{md}^{-1}, \qquad (19)$$

hence its value along the x-axis is 0.525 md^{-1}. All simulations were subjected to steady-state, isothermal, incompressible, Darcian flow in the absence of a gravitational field ($g = 0 \text{ cm/s}^2$), thus, $\Phi = p$. Core porosity was 10%, and the fluid viscosity and density were made to be 1 cp and 1 g/cm^3, respectively. A pressure difference of 1 atm was used ($p_i = 2$ atm; $p_o = 1$ atm).
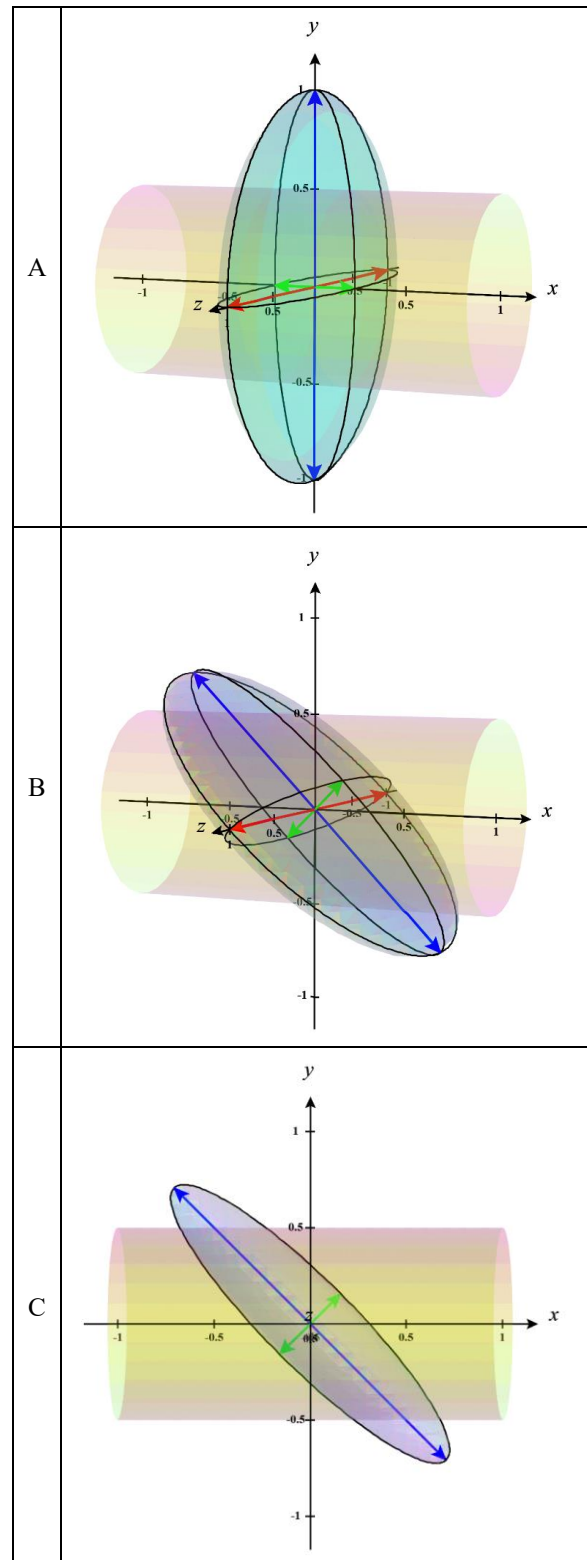
Figure 2. (A) Illustration of a generic cylindrical core and its permeability tensor k_{ij} – geometrically represented as an ellipsoid – initially coordinate-axis-aligned. (B) The permeability tensor (ellipsoid) is rotated +45 degrees about the z-axis. (C) View of the core and representation ellipsoid in the x-y plane. The green arrows (both originating from the origin) represent the maximum principal permeability, $k'_{xx} = 20$ md, which when represented geometrically in the ellipsoid have a magnitude (length) equal to $1/\sqrt{k'_{xx}} = 1/\sqrt{20}$ md$^{-1/2}$. Likewise, the blue and red arrows represent respectively the intermediate and minimum principal permeabilities. See [3], pp.16-19, 26-27, for details.

4 Simulation Results

I. *Should the cylindrical surface of the thin-disc testing (for measuring permeability) be sealed by an impermeable barrier or not*?

To address this question several simulations were conducted in which the outer cylindrical surface of the core was made to be either a no-flow boundary ("sealed") or an open-flow boundary ("not sealed"). Two-dimensional illustrations of these scenarios are given in Figure 3 and example simulation results are given in Figure 4. Further, for a given core length (i.e., thickness), the core diameter was varied to understand how the results change as a function of diameter-to-length ratio. From the simulations the volumetric flow rate Q that exits the outlet planar face of the core, denoted as Q_o, is obtained. With this value the apparent directional permeability is calculated as

$$k_a = Q_o \mu L/(A \Delta p_x). \tag{20}$$

Δp_x is the pressure difference between the inlet and outlet planar faces of the core, i.e., the pressure change that occurs along the x-axis (denoted and calculated as $\Delta p_x = p_{xi} - p_{xo}$). $A = \pi D^2/4$ is the bulk cross-sectional area of the planar face of the core. The "measured" apparent directional permeabilities calculated through Equation (20) are compared to the known ("actual") directional permeability value of 10.5 md in terms of relative percentage error, calculated as

$$\text{Relative Error (\%)} = \frac{100(\text{Meas.} - \text{Act.})}{\text{Act.}} \tag{21}$$

The results of the simulations, in terms of relative percentage error in permeability, are plotted in Figure 5. The following observations are made from Figure 5:

1. For both testing boundary conditions the k_a values measured were always less than the actual permeability value, k_{xx}.
2. For a given core diameter-to-length ratio the k_a values measured for the non-sealed testing boundary condition was always less than the k_a values measured for the sealed testing boundary condition.
3. The k_a values converge towards the actual k_{xx} value when the diameter-to-length ratio was increased.

Considering observation number 2, the reason for the non-sealed scenario to have a relatively larger, negative, error is due to the cross-sectional area assumed and used in the measured permeability value. As qualitatively illustrated in Figure 6, the area A assumed and used in Equation (20) is larger than the actual area perpendicular ($A_\perp$) to the intended pressure gradient vector, thus making the denominator of Equation (20) large and the calculated k_a small. Further, there is fluid flux through the area bordered between $A_\perp$ and A that is being captured for Q_o. However, most of the unit volume of fluid from which this flux originates at the inlet-face bordered between $A_\perp$ and A is exiting the core through the cylindrical surface, thus the value of Q_o is relatively small (relative to the inlet volumetric flow rate Q_i). This, in turn, makes the numerator of Equation (20) small and the calculated k_a small. As the diameter of the core increases, the ratios $A_\perp/A$ and Q_o/Q_i tend toward 1, and k_a tends towards k_{xx} as seen by the relative error tending towards zero in Figure 5. Based on these results it is recommended that the

cylindrical surface of the thin disc be sealed by an impermeable barrier when measuring its permeability.
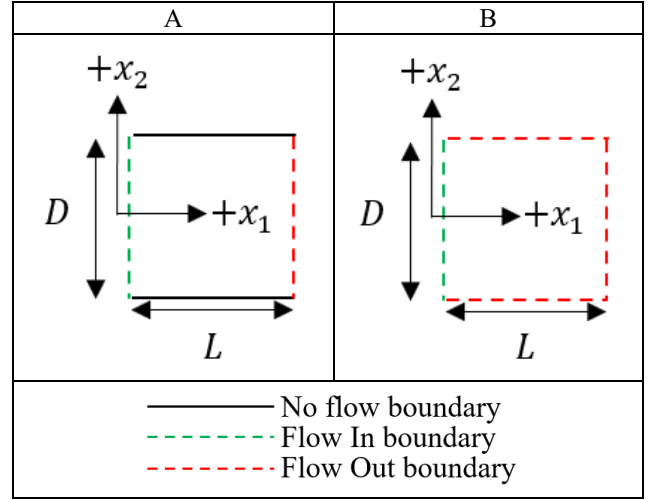
Figure 3. Two-dimensional illustrations of flow boundary conditions for thin-disc permeability measurement, where (A) a no-flow boundary is imposed on the cylindrical surface and (B) an open-flow boundary condition is imposed on the cylindrical surface.

Cylindrical Boundary Sealed		Cylindrical Boundary Not Sealed	
Pressure Contours	Specific Discharge Vector Field	Pressure Contours	Specific Discharge Vector Field
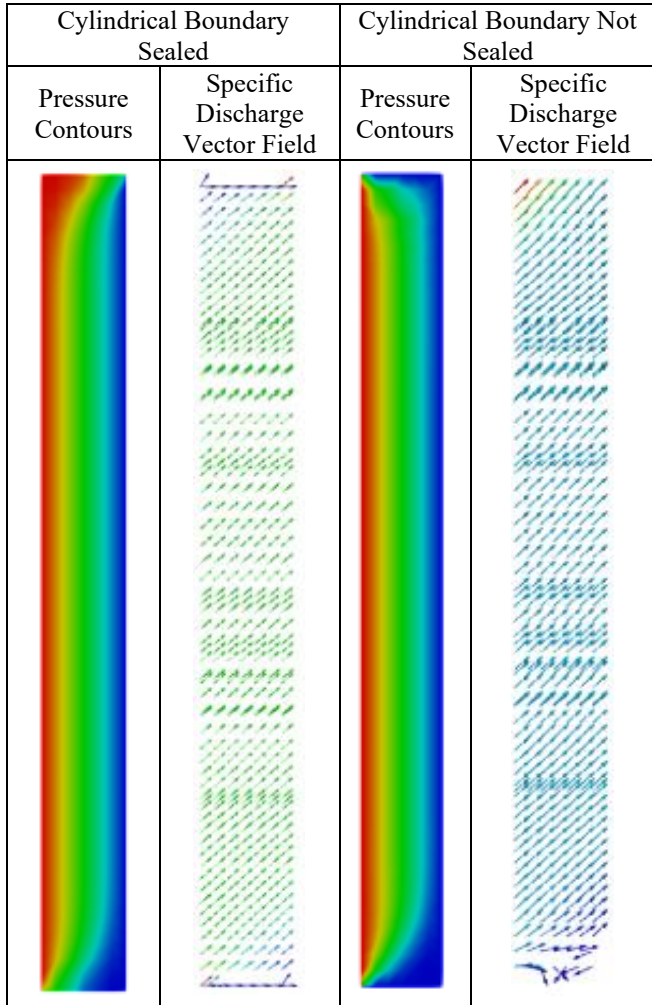
Figure 4. Example thin-disc permeability simulation results for cylindrical boundary sealed (left) and not sealed (right).
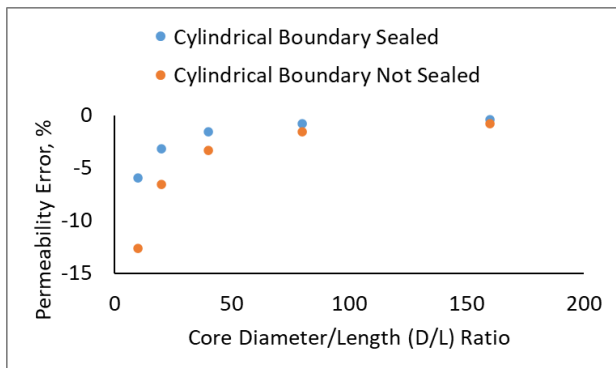
Figure 5. Permeability measurement error for thin-disc simulations with and without core cylindrical boundary sealed.
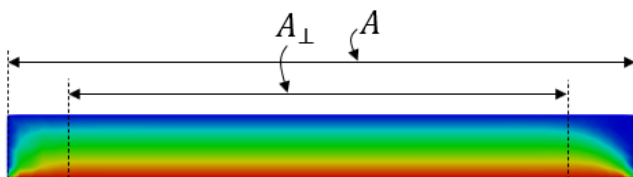
Figure 6. Pressure contours for a thin-disc permeability measurement without the core cylindrical boundary sealed.

II.   *How do the potential contours and specific discharge vector field change as a function of sample dimension*?

To address this question several simulations were conducted with cores having varying D/L ratios and their cylindrical boundary sealed. Figure 7 gives the pressure contours and specific discharge vector fields for cores of varying D/L ratios, from 10 to 1. The upper row in the figure are the pressure contours within the core (red = 2 atm, blue = 1 atm). In the row beneath are the corresponding specific discharge vector fields.
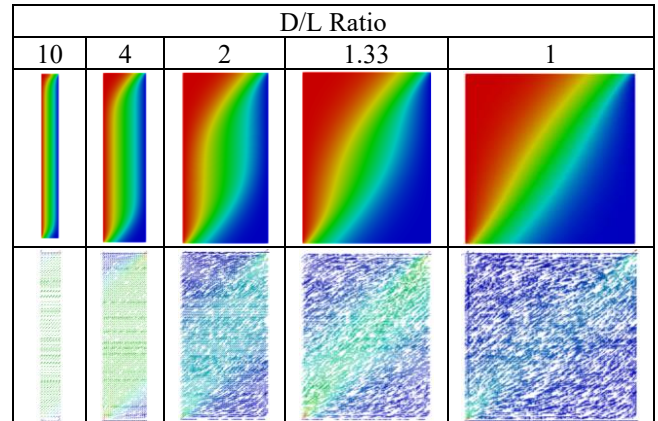
D/L Ratio				
10	4	2	1.33	1

Figure 7. Potential contours and flow velocity fields for cores of varying D/L ratios, from 10 to 1.

As the core D/L ratio is decreased from 10 to 4 the area perpendicular to the prescribed pressure gradient vector decreases. Decreasing the core D/L ratio below 4, towards a ratio of 1, the pressure gradient vector field is distorted; the pressure gradient varies in space, a consequence of overlapping regions affected by the cylindrical edge and planar end effect. For a core geometry of $D/L < 0.5$, the pressure gradient vector field is constant throughout the core (neglecting planar end effects) as seen in Figure 8.

D/L	Pressure Contours and Flow Velocity Vector Field
0.5	
0.25	
0.1	
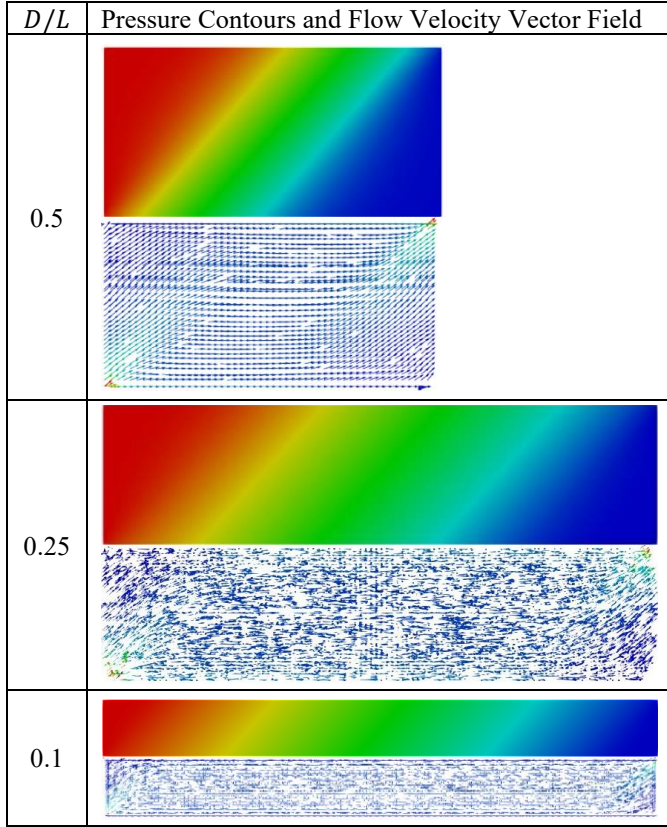
Figure 8. Potential contours and flow velocity fields for cores of varying D/L ratios, from 0.5 to 0.1.

The above results show what has been noted by [23]: the specific discharge vectors are not constant inside the anisotropic sample, and they are systematically oriented in a direction imposed by the principal direction of anisotropy. Similarly, the potential gradient vectors inside an anisotropic sample vary in space. These specific discharge and potential gradient vectors are macroscopic variables — they are pore-volume averages over the porous medium's representative elemental volume (REV). What is measured in experiment are the x_1-direction components of the averaged specific discharge and the averaged potential gradient vectors over the entire sample, and it is these values that are used in Darcy's law to calculate k_a. For these situations where $D/L < 0.5$, the components of the sample-averaged pressure gradient vector can be determined through Equation (8) given that the variables μ, r_{ij}, and $\Delta p_x/L$ are known. The components of the pressure gradient vector are solved for in two steps: 1) Solve for q_1: $q_1 = (-\partial\Phi/\partial x_1)/(\mu r_{11})$; where $(-\partial\Phi/\partial x_1) \approx \Delta p_x/L$. 2) Solve for the other two components of the pressure gradient vector through Equation (8) using the known values of r_{21} and r_{31}. The angle θ at which the pressure gradient vector is oriented in the x-y plane can be computed using

$$\theta = \tan^{-1}\left(\frac{-\partial\Phi/\partial x_2}{-\partial\Phi/\partial x_1}\right) = \tan^{-1}\left(\frac{r_{21}}{r_{11}}\right). \qquad (22)$$

For the three scenarios given above, for $D/L = 0.5, 0.25$, and 0.1, $\theta \cong -42.138°$ (Figure 9).
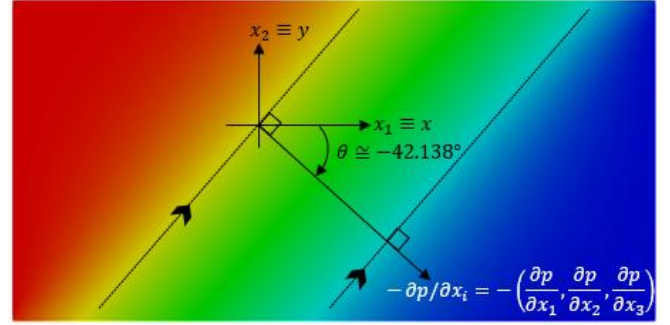
Figure 9. Illustration of the (negative) pressure gradient vector $-\partial p/\partial x_i$ and its orientation angle with the x-axis for the cores simulated having D/L ratios less than 0.5 and their cylindrical boundary sealed.

III. *What dimensions does the sample need to have to yield k with a certain desired accuracy or, more generally, what is the relation between the geometry of a cylindrical sample, expressed by the D/L ratio, and the apparent permeability k_a for a given anisotropy k_{ij} and orientation u_i? How about for viscous resistivity r?*

In the previous section the change in the fluid potential contours and specific discharge vector field as a function of core geometry was examined. In this section we look to see how the apparent permeability and apparent viscous resistivity values change as a function of core geometry for these same simulations. The simulated volumetric flow rates were used to calculate the apparent directional permeability using Equation (20) and the apparent directional viscous resistivity, calculated as

$$r_a = A\Delta p_x/(Q_o\mu L). \qquad (23)$$

The calculated k_a and r_a values are plotted on a semi-log scale in Figure 10. A five-parameter logistic (5PL) function [24], Equation (24), was fitted to the calculated k_a and r_a data and plotted in Figure 10 as dashed curves.

$$y = d + \frac{(a - d)}{(1 + (x/c)^b)^g}. \qquad (24)$$

The parameter values that define these curves are given in Table 1.
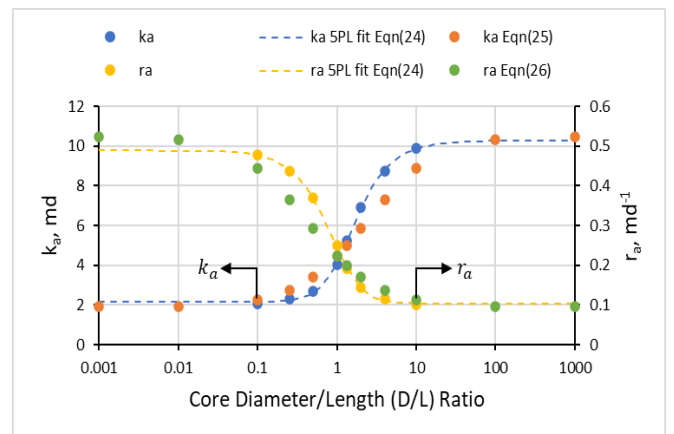
Figure 10. k_a and r_a as a function of core D/L ratio for k_{ij} as defined in Equation (18).

Table 1. 5PL parameters for k_a and r_a.

5PL Curve Fit		
Parameter	k_a	r_a
a	2.16	0.49
b	2.52	1.60
c	1.18	1.46
d	10.28	0.10
g	0.54	2.30

In Equation (24) y is the dependent variable (in this case either k_a or r_a), and x is the independent variable (in this case D/L). The parameter a is the asymptotic value obtained as x tends towards zero. The parameter d is the asymptotic value obtained as x tends towards infinity. See [24] for a detailed description of the roles played by parameters b, c, and g.

The k_a data plotted in Figure 10, whether plotted on a linear-linear, linear-log, or log-log plot, is sigmoidal in shape, monotonically increasing as the core D/L ratio is increased. As indicated by the asymptote parameter d fitted to the k_a data, the best one could do according to the 5PL model fit is measure a permeability value within -2.01% [Equation (21)] of the true k_{xx} value (10.5 md). (The magnitude of this relative error is specific for this permeability tensor's principal values and orientations with respect to the core and core shape (right-circular cylinder)). The inability to measure the true k_{xx} value is due to the edge-effect. In principle, one could eliminate the edge-effect and measure the true k_{xx} value by shaping the cylindrical thin-disc into a rectangular flat-plate and then shaping the edges of the plate to be parallel to the direction taken by q_i at the center of the plate [3] (pp.197-200).

As indicated by the asymptote parameter a fitted to the k_a data, a value as low as 2.16 md could be measured, a -79.4% relative error. Just as the k_a value approaches k_{xx} as the core D/L ratio approaches infinity, the k_a value obtained as the core D/L ratio approaches zero is an approximation of the reciprocal of the true resistivity value $r_{xx} = 0.525$ md^{-1}, which is $1/r_{xx} = 1.905$ md. This result is in accordance with Equation (12).

For the two-dimensional case, using the method of conformal mapping, Marcus [7] solved the problem of determining k_a for any condition of D/L ratio and k_{ij}. Marcus [7] provides the exact solution in the form of equations and graphs. An approximate solution for k_a for the more general three-dimensional case is given by [25],

$$k_a = \sqrt{\frac{k_{ij}u_i u_j}{r_{kl}u_k u_l}} \left[\frac{1 + \sqrt{k_{ij}u_i u_j r_{kl}u_k u_l}(D/L)}{\sqrt{k_{ij}u_i u_j r_{kl}u_k u_l} + (D/L)} \right], \quad (25)$$

and the general approximate solution for r_a is given here,

$$r_a = \sqrt{\frac{r_{kl}u_k u_l}{k_{ij}u_i u_j}} \left[\frac{\sqrt{k_{ij}u_i u_j r_{kl}u_k u_l} + (D/L)}{1 + \sqrt{k_{ij}u_i u_j r_{kl}u_k u_l}(D/L)} \right]. \quad (26)$$

Values for k_a and r_a using these approximate solutions are calculated for the simulation scenarios and plotted in Figure 10 for comparison. As seen, they agree quite well.

Equation (25) shows that k_a is a function of k_{ij} (and inextricably r_{ij}), u_i, D, and L. The simulation results given here is for a specific k_{ij} and u_i, where u_i was defined by α due to the symmetry of the system. Values of k_a for a broader range of values of k_{ij}, u_i, D, and L are given in [7, 26, 23],

which are presented below in Figures 12, 13, and 14, with the approximate solution of [25], Equation (25), superimposed for comparison. In these figures the apparent permeability is normalized to the maximum principal permeability k_1 as a function of the dimensionless parameters $D/L, k_1/k_2$, and α (or their variants L/D and k_2/k_1).
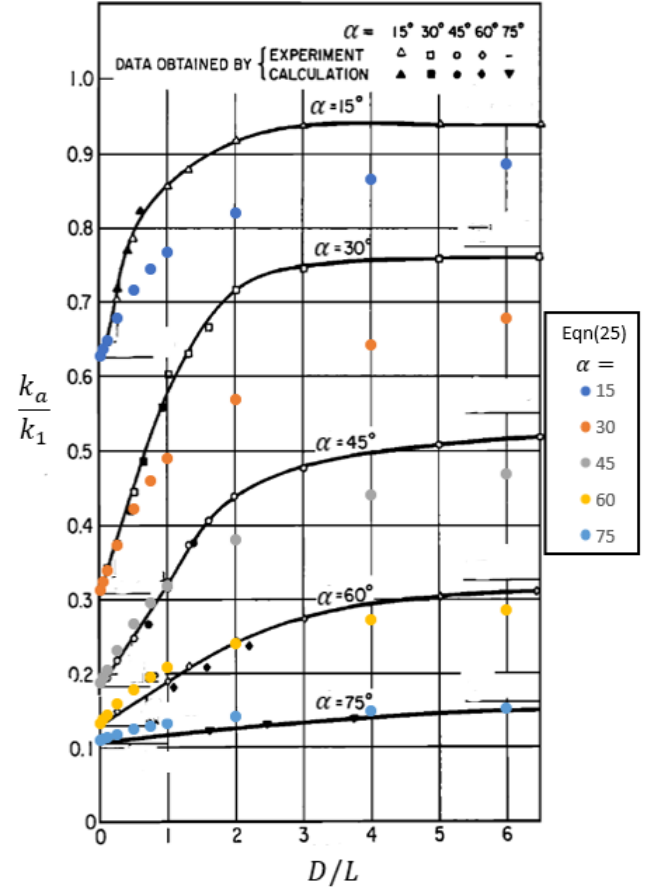
Figure 11. Relation between k_a/k_1 and D/L for $k_2/k_1 = 0.10$ as a function of α (modified and sourced from [7]).
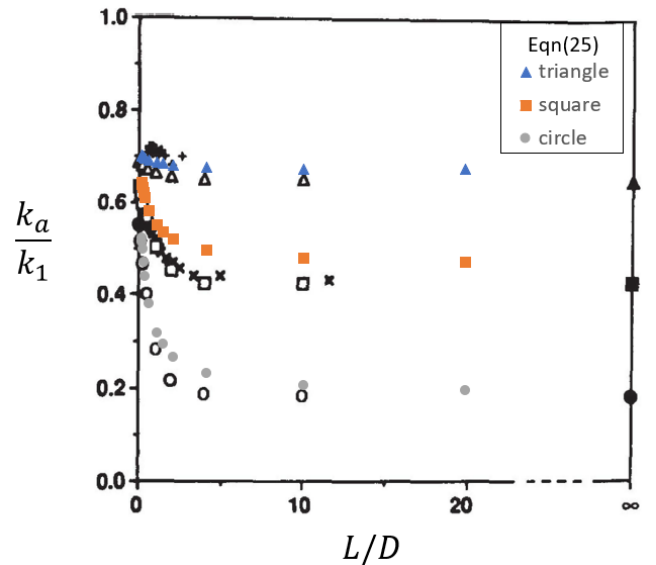
Figure 12. Relation between k_a/k_1 and L/D. Triangles correspond to $k_2/k_1 = 0.6, \alpha = 60°$; squares to $k_2/k_1 = 0.3, \alpha = 45°$; and circles to $k_2/k_1 = 0.1, \alpha = 45°$ (modified and sourced from [26]).
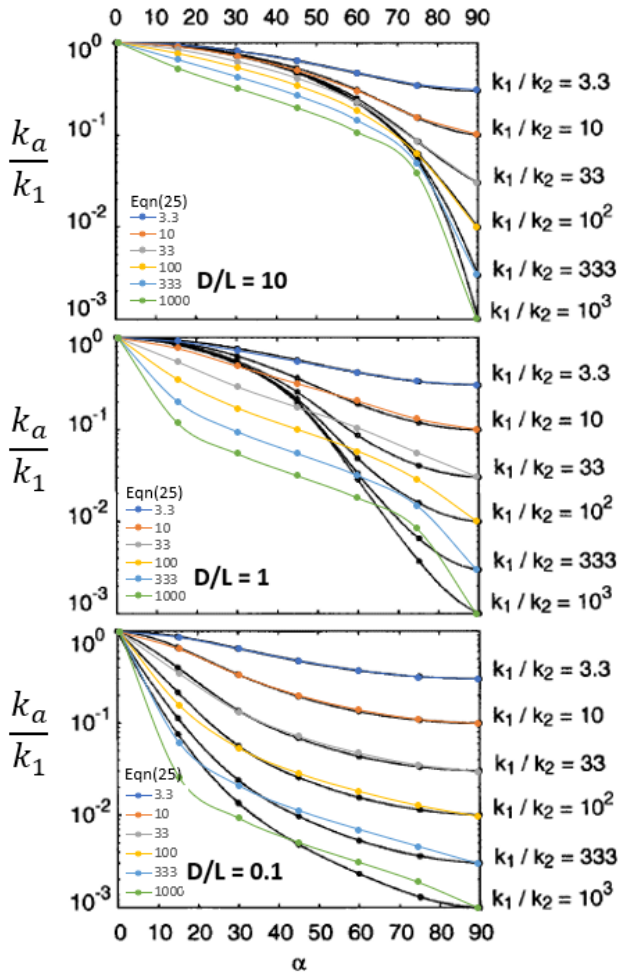
Figure 13. Relation between k_a/k_1, α, and k_1/k_2 for three different D/L ratios: 10 (top), 1 (middle), and 0.1 (bottom) (modified and sourced from [23]).

The accuracy of Equation (25) (and (26)) is measured by the discrepancy between the value it provides, and the values determined through simulation. The data of [7] are from physical simulation using an electrical analog. As noted by [26], there is uncertainty in their experimentally measured values due to the principal permeability directions were not measured directly but inferred. The data of [26] and [23] were derived from numerical simulation, whose accuracy will be a function of iterative convergence error, discretization error, and computer round-off errors. As seen in Figure 13, for $k_1/k_2 \leq 33$, $0.1 \leq D/L \leq 10$, and $0° \leq \alpha \leq 90°$, equation (25) compared quite well, and reasonably well for $k_1/k_2 = 100$. In the author's line of work [5], the largest degree of 3D anisotropy measured to date is $k_{max}/k_{min} = 81.6$ (Figure 14) , and thus equations (25) and (26) will prove to be useful in evaluating the accuracy of experimentally measured k_{ij} and r_{ij}, respectively. (A description of the experiment and analysis to derive the 3D viscous resistivity and permeability tensors shown in Figure 14 is given in a separate paper. See Appendix for a brief description.)

$$r_{ij}(x,y,z) = \begin{bmatrix} 1.07 & -0.20 & -0.12 \\ -0.20 & 0.06 & 0.01 \\ -0.12 & 0.01 & 0.05 \end{bmatrix} md^{-1}$$

$$r'_{ij}(x',y',z') = \begin{bmatrix} 1.12 & 0 & 0 \\ 0 & 0.05 & 0 \\ 0 & 0 & 0.014 \end{bmatrix} md^{-1}$$

$$k_{ij}(x,y,z) = \begin{bmatrix} 4 & 13 & 6 \\ 13 & 62 & 17 \\ 6 & 17 & 29 \end{bmatrix} md$$

$$k'_{ij}(x',y',z') = \begin{bmatrix} 0.09 & 0 & 0 \\ 0 & 21.5 & 0 \\ 0 & 0 & 72.7 \end{bmatrix} md$$
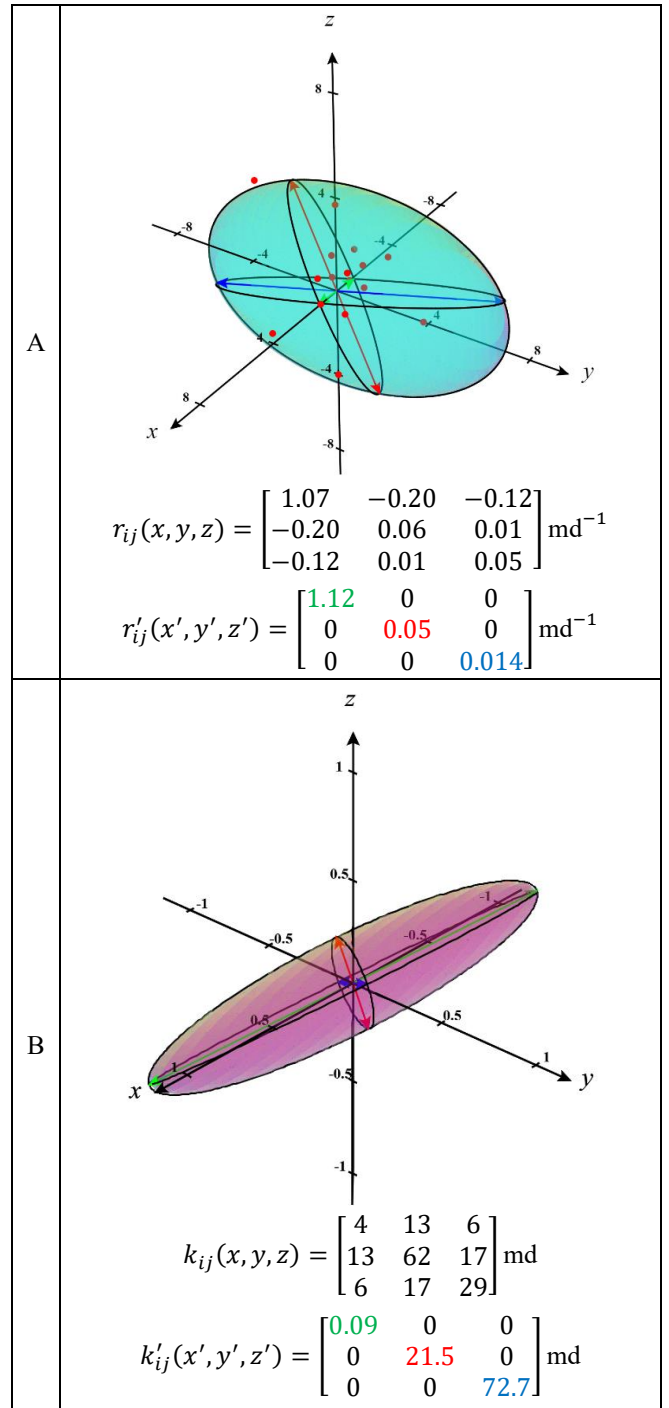
Figure 14. A) Experimentally measured directional viscous resistivity values (red points), best-fit viscous resistivity tensor r_{ij} to the measured values -- geometrically represented as an ellipsoid, and principal viscous resistivity values and axes (arrows). B) Permeability tensor k_{ij} derived from the viscous resistivity measurements. Note, to maintain parity the viscous resistivity principals are listed as $r_1 > r_2 > r_3$ and therefore the permeability principals are listed as $k_1 < k_2 < k_3$.

5 Summary

Darcy's law is considered the fundamental law of fluid motion in porous media. The relationships embodied in Darcy's law form the necessary basis upon which any analytical theory of fluid motion through porous media must rest [27] (p.792). Darcy's law defines permeability, the basic

flow property of a porous medium, and is "probably the most important single physical property of oil and gas sands" (George Fancher in [28]). Darcy's law is meaningless unless the numerical values of the permeability coefficients appearing in it can be determined [4] (p.148). Permeability is a *parameter of ignorance*, and in practice must be deduced from actual experiments [4] (p.25). In this paper the mathematical theory and physical underpinnings of a permeability experiment have been explored.

It is shown that in the general and likely case of an anisotropic medium that is to be measured, and the measurement orientation is not along one of the principals, a sample with a D/L ratio $\gg 1$ is to be used if permeability is to be measured; and $D/L \ll 1$ if viscous resistivity is to be measured. Since permeability and viscous resistivity are second-rank tensors, the values measured in experiment are apparent scalar directional values. This means that for a permeability experiment, which is measured using the "thin disc" geometry with the cylindrical surface sealed, an apparent permeability in the direction of the potential gradient is measured. The value is labelled "apparent" because the directional permeability is only approximately in the direction of the sample-averaged potential gradient vector, which is due to end/edge-effects caused by the sample's right-circular cylindrical shape and imposed boundary conditions. The degree to which the apparent value for the measured directional permeability k_a (or viscous resistivity r_a) differs from the true value is a function of $k_{ij}, r_{ij}, u_i, D,$ and L. This relationship has been explored and approximate analytical solutions for k_a and r_a as function of $k_{ij}, r_{ij}, u_i, D,$ and L have been provided, which can be used to guide choice of experimental setup, "thin-disc" or "long rod", and to approximate measurement accuracy (in addition to standard measurement error analysis). It is noted that end/edge-effects may be eliminated, in principle, if the samples are shaped as described in [3] (pp.199-200).

The term "permeability" is defined by Darcy's law, which refers to the magnitude of the fluid potential gradient vector and the component of the specific discharge vector collinear with it. Therefore, the unit of permeability is defined by Darcy's law: a material has a *directional permeability* of one darcy if through a face of one square centimeter, *which is normal to the direction of the potential gradient*, one cubic centimeter per second of fluid having viscosity one centipoise is caused to flow by a potential gradient of one atmosphere per centimeter.

For experiments employing "long rod"-like sample dimensions ($D/L \sim 0.5$), such as those used by Darcy and as recommended in recent literature [18, 19, 10], values for apparent viscous resistivity in the direction of flow should be measured. As shown, the smaller the D/L ratio is the more accurate the r_a value is to the true r_q. In the general case where the orientations of principal permeabilities for the sample being measured are not known, one should not try to directly determine values for k_{ij} when using the "long rod" experiment ($D/L \ll 1$). Instead, measure six or more values of r_a (see Appendix), determine values for r_{ij} and either use these values in the viscous resistivity form of Darcy's law, or determine k_{ij} by taking the reciprocal of r_{ij} and using these k_{ij} in the permeability form of Darcy's law. Example results of this procedure has been shown, where the three-

dimensional resistivity tensor was measured from several r_a measurements, from which the three-dimensional permeability tensor was determined.

Nomenclature

The text is written in an indicial notation whereby quantities with a single index represents components of vectors, and quantities with two subscripts are components of second rank tensors. Letter indices i, j, etc., stand collectively for the integer number subscripts 1, 2, or 3. Indices 1, 2, 3, correspond respectively to Cartesian coordinate system axes x, y, z. Einstein summation convention is used. Where the context prevents confusion with a scalar, the magnitude of a vector a_i or tensor S_{ij} quantity is denoted by non-indexed variable, e.g., a and S, respectively. Where the context prevents confusion with a vector, principal values of second-rank tensors are designated with a single subscript, e.g., $S_1, S_2,$ and S_3, with the convention, $S_1 \geq S_2 \geq S_3$.

a_i = flux or effect vector
A = bulk cross-sectional area of the planar face of the cylindrical core, L^2
$A_\perp$ = actual bulk cross-sectional area perpendicular to the intended pressure gradient vector as illustrated in Figure 6, L^2
b_i = force or gradient or cause vector
c = trigonometric function cosine
D = diameter, L
g = acceleration due to gravity, LT^{-2}
h = hydraulic head or piezometric head, defined as $\frac{p}{\rho g} + z, L$
J_i = hydraulic gradient vector, defined as $-\partial h/\partial x_i$, dimensionless
k_{ij}, k = permeability, L^2
K_{ij}, K = hydraulic conductivity, LT^{-1}
k_a = the apparent directional permeability of a finite-dimensioned sample in the u_i direction measured using a conventional axial permeameter, L^2
k_Φ = permeability in the direction of the fluid potential gradient, L^2
k_q = permeability in the direction of flow, L^2
m_i = unit vector in the direction of the specific discharge vector
n_i = unit vector in the direction of the negative of the potential gradient vector
L = length, L
p = fluid pressure, $ML^{-1}T^{-2}$
p_i, p_o = core inlet and outlet fluid pressures, respectively, $ML^{-1}T^{-2}$
Δp_x = the fluid pressure difference between the inlet and outlet planar faces of the core, $ML^{-1}T^{-2}$
q_i = specific discharge vector (volumetric flux), LT^{-1}
Q = volumetric flow rate, $L^3 T^{-1}$
Q_i, Q_o = volumetric flow rate that passes through the inlet and outlet planar faces of the core, respectively, $L^3 T^{-1}$
r_{ij}, r = viscous resistivity, L^{-2}
r_a = the apparent directional viscous resistivity of a finite-dimensioned sample in the u_i direction measured using a conventional axial permeameter, L^{-2}
r_q = viscous resistivity in the direction of flow, L^{-2}

R_{ij}, R = hydraulic resistivity, $L^{-1}T$

R_{ij} = rotation matrix

s = trigonometric function sine

S_{ij} = symmetrical second-rank tensor

u_i = unit vector in the specific direction for which the magnitude of a second-rank tensor is sought.

x_i = general Cartesian coordinate, or component, final position vector, $(x_1, x_2, x_3) \equiv (x, y, z)$.

x_i = right-handed Cartesian coordinate system axes, $x_1 \equiv x, x_2 \equiv y, x_3 \equiv z$. The z-axis is vertical and positive upward, and colinear with gravitational acceleration vector g_i $(0, 0, g)$.

x_i' = right-handed Cartesian coordinate system axes aligned with the principal axes of the tensor. The axes x_i and x_i' have the same origin.

z = elevation of the point at which the piezometric head is being considered in reference to some datum level, L

α = angle between the maximum principal permeability axis and the core's symmetry axis, dimensionless

θ = angle, dimensionless

θ, ϕ, ψ = rotation angles as used in Equation (16), dimensionless

μ = dynamic viscosity, $ML^{-1}T^{-1}$

ρ = volumetric mass density, ML^{-3}

Φ = fluid potential, defined as $p + \rho g z$, $ML^{-1}T^{-2}$

Works Cited

1. H.P. Darcy, *Les Fontaines Publiques de la ville de Dijon* (1856).

2. J. Ferrandon, Genie Civil, *125*(2), 24-28, (1948).

3. J. F. Nye, *Physical Properties of Crystals: Their Representation by Tensors and Matrices* (1985).

4. J. Bear, *Dynamics of Fluids in Porous Media.* (1988).

5. J.A. McGregor, J. Int. Perf. Forum, *II*(1), 22-59 (2018).

6. H. Marcus, D.E. Evenson, *Directional Permeability in Anisotropic Porous Media.* (1961).

7. H. Marcus, J. Geophys. Res., *67*(13), 5215-5225 (1962).

8. D.R. Lovett, *Tensor Properties of Crystals* (2017).

9. R.E. Newnham, *Properties of Materials: Anisotropy, Symmetry, Structure.* (2005).

10. API. *Recommended Practices for Core Analysis* (1998).

11. J. Hagoort, *fundamentals of gas reservoir engineering* (1988).

12. A.E. Scheidegger, Geofys. Pura Appl., *28*(1), 75-90 (1954).

13. A.E. Scheidegger, *The Physics of Flow Through Porous Media.* (1957).

14. H.S. Carslaw, J.C. Jaeger, *Conduction of Heat in Solids* (1959).

15. R.E. Collins, *Flow of Fluids Through Porous Materials.* (1961).

16. G.O. Brown, Water Resour. Res., *38*(7), 11:1-12. (2002).

17. G. Brown, *Summary of Darcy's Experiments.* (2000)

18. ASTM D4525. Standard Test Method for Permeability of Rocks by Flowing Air. (2013).

19. C. McPhee, J. Reed, I. Zubizarreta, *Core Analysis: A Best Practice Guide.* (2015).

20. P.A. Rice, D.J. Fontugne, R.G. Latini, A.J. Barduhn, Ind. and Eng. Chem., *62*(6), 23-31 (1970).

21. B. McGinty, *Rotation Matrices.* (2012).

22. H. Goldstein, C. Poole, J. Safko, *Classical Mechanics* (2001).

23. P. Renard, A. Genty, F. Stauffer, J. Geophys. Res., *106*(B11), 26,443-26,452 (2001).

24. P.G. Gottschalk, J.R. Dunn, Anal Biochem (343), 54-65. (2005).

25. M.N. Dmitriev, N.M. Dmitriev, V.V. Kadet, M.N. Kravchenko, S.G. Rassokhin, Fluid Dyn., *39*(4), 589-593 (2004).

26. Y. Bernabé, In B. Evans, & T.-f. Wong, *Fault Mechanics and Transport Properties of Rocks* (pp. 147-167). (1992).

27. M.K. Hubbert, J. Geol., *48*(8), 785-944 (1940).

28. L.J. Klinkenberg, Drill. & Prod. Pract., 200-213 (1941).

Appendix

The 3D symmetric viscous resistivity tensor r_{ij} contains nine components, six of which are independent. To retrieve these six components, one needs at least six independent directional viscous resistivity measurements in independent directions. A regression analysis to these measurements is then performed to determine the values of r_{ij}. It is more accurate to measure more than six independent apparent directional viscous resistivities and combine these observations to give the best value of r_{ij}. The same can be said for the 3D symmetric permeability tensor k_{ij}, where six or more independent directional permeability measurements are required to be analyzed. Since the symmetric r_{ij} and k_{ij} tensors are reciprocals of each other, the experimentation for- and determination of- only one tensor is required, and the other tensor can be found immediately by computing its reciprocal (matrix inverse). The accuracy of the six tensor components determined will be a function of the accuracy of directional measurements. The accuracy of the individual apparent directional permeability measurements increases as the D/L ratio of the samples is increased. The accuracy of the individual apparent directional viscous resistivity measurements increases as the D/L ratio of the samples is decreased.